Organosulfates from Dark Aqueous Reactions of Isoprene-Derived Epoxydiols Under Cloud and Fog Conditions: Kinetics, Mechanism, and Effect of Reaction Environment on Regioselectivity of Sulfate Addition

Sarah S. Petters,* Tianqu Cui, Zhenfa Zhang, Avram Gold, V. Faye McNeill, Jason D. Surratt, and Barbara J. Turpin

Read Online

ACCESS | Metrics & More | Article Recommendations | Supporting Information

ABSTRACT: Atmospheric oxidation of isoprene yields large quantities of highly water-soluble isoprene epoxydiols (IEPOX) that partition into fogs, clouds, and wet aerosols. In aqueous aerosols, the acid-catalyzed ring-opening of IEPOX followed by nucleophilic addition of inorganic sulfate or water forms organosulfates and 2-methyltetrols, respectively, contributing substantially to secondary organic aerosol (SOA). However, the fate of IEPOX in clouds, fogs, and evaporating hydrometeors is not well understood. Here we investigate the rates, product branching ratios, and stereochemistry of organosulfates from reactions of dilute IEPOX (5−10 mM) under a range of sulfate concentrations (0.3−50 mM) and pH values (1.83−3.38) in order to better understand the fate of IEPOX in clouds and fogs. From these aqueous dark reactions of β-IEPOX isomers (*trans-* and *cis*-2-methyl-2,3-epoxybutane-1,4-diols), which are the predominant IEPOX isomers, products were identified and quantified using hydrophilic interaction liquid chromatography coupled to an electrospray ionization high-resolution quadrupole time-of-flight mass spectrometer operated in negative ion mode (HILIC/(−)ESI-HR-QTOFMS). We found that the regiochemistry and stereochemistry were affected by pH, and the tertiary methyltetrol sulfate ($C_5H_{12}O_7S$) was promoted by increasing solution acidity. Furthermore, the rate constants for the reaction of IEPOX under cloud-relevant conditions are up to 1 order of magnitude lower than reported in the literature for aerosol-relevant conditions due to a markedly different solution activities. Nevertheless, the contribution of cloud and fog water reactions to IEPOX SOA may be significant in cases of lower aqueous-phase pH (model estimate) or during droplet evaporation (not studied).
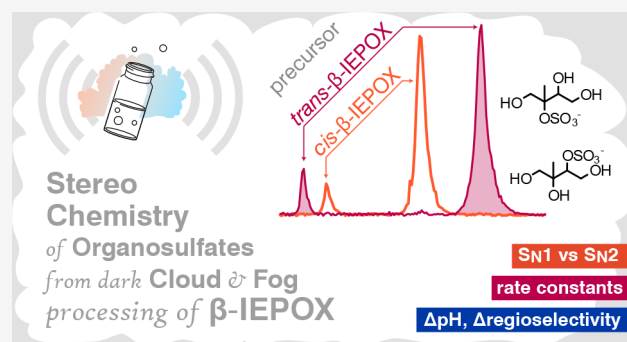
1. INTRODUCTION

Aerosols are an important link between the land surface and atmosphere, affecting the global climate mainly through their indirect effects on clouds[1,2] and public health through reduced air quality.[3,4] A large fraction of aerosol mass is organic, formed mostly through atmospheric chemistry.[5] Isoprene is the dominant non-methane hydrocarbon emitted by the biosphere, accounting for about half of the roughly 1000 Tg yr^{-1} of carbon produced globally by plants.[6] Isoprene reacts readily with OH radicals in the sunlit atmosphere,[7] producing a high yield of isoprene-derived epoxydiols (IEPOX) under low-nitric oxide (NO) conditions.[8,9] These and other isoprene oxidation products serve as important precursors to secondary organic aerosol (SOA) formation through acid-catalyzed multiphase reactions[10,11] and therefore should be considered explicitly in large-scale atmospheric chemistry models.[12−15]

Between 17 and 40% of the organic fraction of ambient aerosol mass is traceable to reactions of IEPOX in areas of high isoprene emission, such as the Southeast United States,[14,16−21] the Amazon Rainforest,[22,23] or Southeast Asia.[16−18,22,24,25] The most abundant IEPOX isomers are *trans-β*-IEPOX (∼64%), *cis-β*-IEPOX (∼32%), and δ1-IEPOX (<3%).[26] In acidified sulfate solutions, β-IEPOX isomers (*trans-* and *cis*-2-methyl-2,3-epoxybutane-1,4-diols) undergo irreversible ring-opening reactions yielding predominantly tetrols (2-methyltetrol diastereomers; 2-MTs) and organosulfates (methyltetrol sulfate diastereomers; MTSs).[10] The 2-MTs, 2-methylthreitol, and 2-methylerythritol are detected in large quantities in ambient fine aerosol ($PM_{2.5}$) and are tracers for isoprene-

Scheme 1. Reaction of *trans*-β-IEPOX with Acidic Sulfate by A-1 (Top), A-2 (Middle) or General Acid (Bottom) Mechanisms[a]
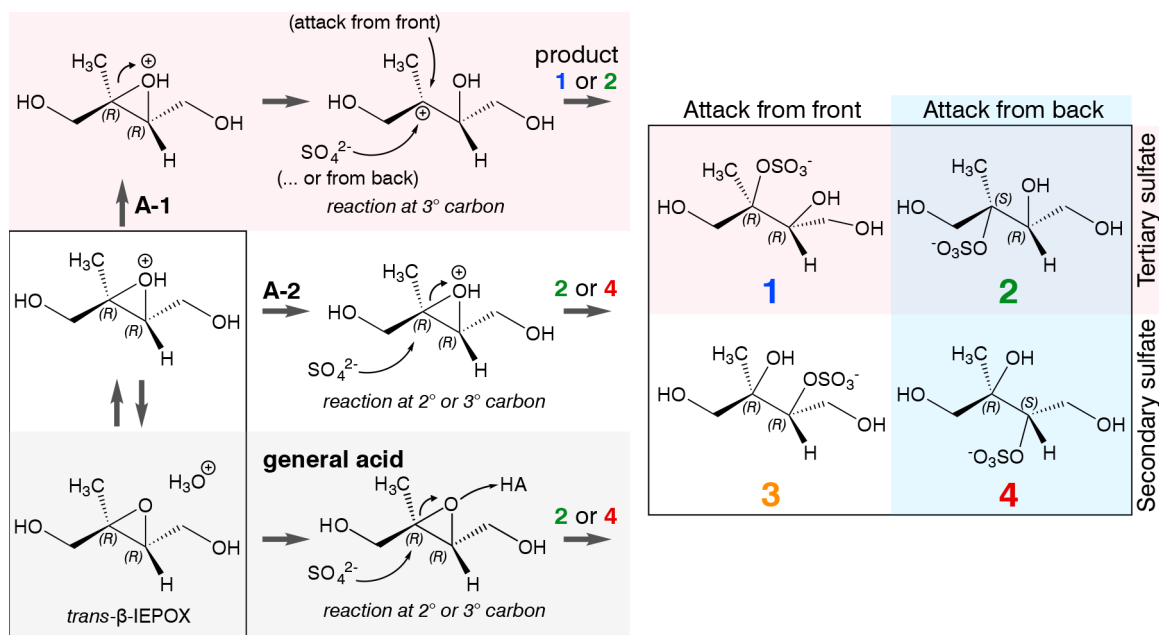
[a]Products 1−4 are shown to the right; product 3 is only expected from the reaction of *cis*-β-IEPOX (not shown).

derived SOA in areas of high isoprene activity.[27−30] Recent efforts to speciate and quantify 2-methyltetrol sulfate diastereomers (2-MTSs) in anthropogenically influenced isoprene-rich areas have shown 2-MTSs to be the single most abundant SOA constituent in $PM_{2.5}$, contributing 10−13% of organic carbon in thse Southeast United States and Manaus, Brazil,[31,32] as well as up to 15% of organic carbon during the 2017 Lake Michigan ozone study.[33] Understanding the impact of the changing anthropogenic influence on reaction pathways is critical for isoprene-derived SOA.[11,34,35]

Multiphase reactions of IEPOX are facilitated by the high solubility of IEPOX in water and the high concentrations of gas-phase IEPOX in source regions during photochemically active periods. Summertime surface-level IEPOX concentrations range from 0.35 to 1.0 ppb in the Southeastern United States[14,15] and up to 0.2 and 1.6 ppb at 1 km above the surface in the Western and Eastern United States, respectively.[36] Much of what we know about IEPOX SOA is from acid-catalyzed reactions occurring in aerosols. Lifetimes against gas-phase photochemical degradation are 1.4−2.8 h for isoprene[37,38] and 1.6 h for IEPOX,[13] giving the unreacted species ample time to reach the cloud layer in a typical convective boundary layer with a mixed-layer turnover time of 10−15 min.[39] Partitioning into cloudwater results in dilute solutions and slower reaction rates, but cloud and fogwater, when present, represent a much higher total surface area and water volume for gas-to-particle partitioning than do aerosols.[40] Dissolved organic carbon has long been detected in fogs and clouds, indicating the potential for dilute aqueous solutions to result in appreciable aerosol mass after water evaporation.[41−43] Cloud chemistry studies have focused on the quantification of carboxylic acids and carbonyls[43−45] resulting from the oxidation of glyoxal, methylglyoxal, and pyruvic acid,[46−49] but recent work indicates that epoxides, including IEPOX, may also serve as precursors to the production of low-volatility species in cloudwater.[50,51] IEPOX is relatively water-soluble; estimates of the Henry's Law constant for IEPOX range from 2.7×10^6 to 1.7×10^8 M

atm^{-1},[15,52−56] rivaling those of glyoxal, methylglyoxal, and pyruvic acid, whose Henry's Law constants are $0.36−50 \times 10^6$,[57−61] $0.35−3.2 \times 10^4$,[60−62] and 3.1×10^5 M atm^{-1},[61,63−65] respectively. Organosulfates have been detected in cloud and fog waters, as well as in precipitation (rain, snow, and hail),[45,66−70] including abundant 2-MTS isomers, observed by electrospray ionization mass spectrometry (ESI-MS) as deprotonated ions at mass-to-charge ratios (m/z) 215, specifically attributable to IEPOX-derived MTSs,[67,68] prompting a question as to whether cloud/fog processing could be a source of IEPOX-derived organosulfates. Although much of the knowledge of IEPOX-derived MTSs originates from chamber and flow tube studies using acidified aerosols,[10,71] aerosol formation from IEPOX measured during field campaigns does not universally trend with estimates of aerosol acidity.[17,18] This also highlights the possibility of cloudwater formation of IEPOX SOA and has prompted recent studies of acid-catalyzed IEPOX reactions modeled at cloud-relevant aqueous concentrations[50] and experimental OH radical-initiated aqueous oxidation of IEPOX.[72] Here we extend these studies by investigating dark acid-catalyzed reactions of *trans*- and *cis*-β-IEPOX, in acidified sulfate solutions at fog and cloud-relevant concentrations.

Differentiation between isomers of IEPOX-derived 2-MTs and MTSs is possible for ambient aerosols using a recently developed hydrophilic interaction liquid chromatography coupled to electrospray ionization high-resolution quadrupole time-of-flight mass spectrometry (HILIC/ESI-HR-QTOFMS) method.[31,73] Enhancement of one isomer over another can indicate the relative contribution of a specific mechanism. For example, Nozière et al.[29] used the enhancement of one 2-MT diastereomer as a tracer for isoprene-derived tetrols in ambient aerosols. The distribution of isomers formed in reactions of IEPOX elucidates details of the mechanism of substitution at asymmetric carbons C2 and C3,[52,74] and identifying the mechanistic underpinnings can enable predictive frameworks for shifts in distribution under different conditions.[75] The

stability, hygroscopicity, solubility, viscosity, and volatility of 2-MT and MTS isomers is controlled by structural differences as well as functional groups.[73,76−82] Here we apply our recently developed HILIC/ESI-HR-QTOFMS method[31] to investigate product distributions under differential reaction conditions relevant to cloud and fog waters.

2. EXPERIMENTAL SECTION

2.1. Standards. Authentic standards of racemic *trans-β*-IEPOX, *cis-β*-IEPOX, 2-MTs, and MTSs were synthesized as described in previous work.[31,83,84] Four MTS isomers in the standard mixture are shown as Products 1−4 in Scheme 1. Pure standards were stored neat at −20 °C until use. For quantification, 2 mg mL^{-1} standards were prepared in Milli-Q water and diluted into 95:5 (v/v) acetonitrile (ACN, HPLC grade, Fisher Scientific)/Milli-Q H$_2$O mixture at 10, 5, 2.5, 1, 0.1, 0.01 μg mL^{-1}, and 95:5 v/v ACN:Milli-Q served as a solvent blank.

2.2. Dark Aqueous Experiments. *trans-* or *cis-β*-IEPOX was added to aqueous acidified sulfate in glass reactors to determine the branching ratio between 2-MTs and MTSs, reaction rates, and distribution of isomeric products as a function of pH and sulfate concentration, as detailed in Table 1. Samples were generated in 4 mL batches in precleaned

Table 1. Experiments Conducted[a]

#	IEPOX	sulfate[b]	pH[c]	H$_2$SO$_4$	(NH$_4$)$_2$SO$_4$
1	5	5	2.32	5	0
2	5	5	1.83	5	0
3	5	5	2.25	2.32	2.68
4	5	5	2.55	1.08	3.92
5	5	5	3.16	0.5	4.5
6	5	5	3.22	0.5	4.5
7	5	5	3.16	0.5	4.5
8	5	5	3.00	0.5	4.5
9	5	6.67	3.10	0.5	6.17
10	5	8.33	3.13	0.5	7.83
11	5	10	3.17	0.5	9.5
12	5	50	3.38	0.5	49.5
13	5[d]	5	2.79	0.5	4.5

[a]Values are expressed in mmol L^{-1} and are derived from reactant quantities added to mixture. IEPOX was added at $t = 0$ min. [b]Sum of H$_2$SO$_4$ and (NH$_4$)$_2$SO$_4$ concentrations. See Table 2 for activities of HSO$_4^-$ and SO$_4^{2-}$. [c]pH recorded after addition of IEPOX using a pH probe accurate to 0.01 pH units (Denver Instruments UltraBasic-10) that was cleaned and calibrated at pH 2, 4, 7, and 10 before each measurement. [d]This experiment used *cis-β*-IEPOX. All others used *trans-β*-IEPOX.

borosilicate glass scintillation vials by mixing 5 mM IEPOX in water with (NH$_4$)$_2$SO$_4$ and H$_2$SO$_4$ to provide 5−50 mM total added sulfate (HSO$_4^-$ + SO$_4^{2-}$). The concentration of IEPOX in cloudwater is close to the experimental value we used and can be estimated from field and lab measurements of gas-phase IEPOX[14,15,36] and its Henry's law constant.[52−55] Using approximate values of 1 ppb and 10^7 M atm^{-1} results in an IEPOX cloudwater concentration of 10 mM. Results from the GAMMA 5.0 model[50,85,86] indicate that concentrations of dissolved IEPOX in cloudwater may range from 4 to 8 mM in areas of high isoprene activity, such as the Whiteface Mountain Observatory and during the Southern Oxidant and Aerosol Study SOAS in 2013.[6] The total added sulfate in this work is

roughly 1 order of magnitude higher than that of continental cloudwater;[87] this was necessary to accelerate the reaction, enabling us to quantify the reaction rate and to control the pH through addition of H$_2$SO$_4$. One experiment at pH 5 was conducted at low sulfate concentration (300 μM), with higher IEPOX concentration (10 mM) to speed up the reaction and enable determination of the rate. The sulfate concentration is comparable to that measured in continental cloudwater (up to 100 μM sulfate).[87] The ratio (NH$_4$)$_2$SO$_4$ to H$_2$SO$_4$ was adjusted to control pH between 1.83−3.38, consistent with fog or polluted cloudwater.[87,88] Solution pH was measured using a pH probe (Denver Instruments UltraBasic-10) accurate to 0.01 pH units. pH was not observed to change during the reaction.

IEPOX is highly reactive, and care was taken to time the experiments accurately. Sulfate solutions were prepared first. Authentic standards of *trans-* or *cis-β*-IEPOX were diluted in Milli-Q water within 2 min of initiating the reactions, and then IEPOX was added to sulfate ($t = 0$). Aliquots were removed and diluted in ACN to 95:5 v/v ACN/H$_2$O to slow the reaction. The reaction time for each sample was recorded at the instant of dilution using a stopwatch. Dilute samples were stored at −20 °C for <24 h before analysis. Repeated injections with varying storage times provided consistent results and confirmed that this procedure slowed the reaction sufficiently to prevent measurable changes after aliquot collection.

Table 2 shows the activities of all species in the solution, estimated using the Extended Aerosol Inorganics Model (E-AIM; www.aim.env.uea.ac.uk; Model III).[89,90] Activity coefficients are included in the Supporting Information (SI) in Table S1. Solutions were composed of NH$_4^+$, SO$_4^{2-}$, HSO$_4^-$, H$_2$O, OH$^-$, H$_3$O$^+$, and IEPOX.

2.3. Quantification of Products Using HILIC/(−)ESI-HR-QTOFMS. Total 2-MTs and MTSs were quantified by HILIC/ESI-HR-QTOFMS operated in the negative (−) ion mode as described previously.[31] Separation was achieved using an Agilent 1200 series HPLC system with a Waters Acquity UPLC ethylene bridged hybrid amide (BEH) column (2.1 × 100 mm, 130-Å pore size, 1.7-μm particle size) without a guard column at 35 °C and an elution rate of 0.3 mL min^{-1}. The mobile phase consisted of Milli-Q water (mobile phase A) and 95:5 (v/v) acetonitrile/Milli-Q H$_2$O (mobile phase B), both with 13 mM ammonium acetate and adjusted to pH 9 using ammonium hydroxide. A 30 min gradient elution in mobile phase A was as follows: 0% for 4 min; ramp to 15% from 4 to 20 min; held constant at 15% between 20 and 24 min; ramp down to 0% from 24 to 25 min; and held constant at 0% from 25 to 30 min. The sample injection volume was 5 μL, and all samples were in a 95:5 (v/v) ACN/Milli-Q H$_2$O solvent mixture. Calibration and tuning of the QTOF were performed as described previously,[31] and mass resolution ranged from 11000−21000 for calibrant masses of m/z 112−1600.

The extracted ion chromatograms (EICs) in Figure 1 show the chromatographic separation of 2-MT and MTS isomers. The 2-MT diastereomers, 2-methylthreitol and 2-methylery-thritol, co-elute (m/z 135.066, C$_5$H$_{11}$O$_4^-$). Synthesis of the MTS standard yields four isomers that can be chromatographically resolved by the HILIC/ESI-HR-QTOFMS method (m/z 215.023, C$_5$H$_{11}$O$_7$S$^-$). Because the tertiary isomers were the synthetic targets and the secondary isomers were minor byproducts, major peaks C and D can be identified as tertiary MTSs (2-MTS, or 1,3,4-trihydroxy-2-methylbutan-2-yl sulfate) and minor peaks A and B as the secondary MTSs (3-MTS, or

Table 2. Activities of Ions in Solution[a]

#	NH_4^+ (mmol L^{-1})	HSO_4^- (mmol L^{-1})	SO_4^{2-} (mmol L^{-1})	OH^- (pmol L^{-1})	NH_3 (nmol L^{-1})
1	0.00	1.49	2.10	1.35	0.00
2	0.00	1.49	2.10	1.35	0.00
3	4.75	0.80	2.53	3.03	0.82
4	6.94	0.40	2.77	6.68	2.63
5	7.94	0.19	2.90	14.56	6.57
6	7.94	0.19	2.90	14.56	6.57
7	7.94	0.19	2.90	14.56	6.57
8	7.94	0.19	2.90	14.56	6.57
9	10.70	0.22	3.63	15.65	9.51
10	13.40	0.25	4.29	16.65	12.66
11	16.04	0.27	4.91	17.59	16.04
12	71.62	0.40	13.57	32.68	133.00
13[b]	7.94	0.19	2.90	14.56	6.57

[a]Activity = concentration × activity coefficient/$c^\ominus$, where $c^\ominus$ is the reference unit of concentration included in the heading. Table S1 gives activity coefficients for these mixtures. Values are obtained using E-AIM. Activity of water is 55.51 (mol L^{-1}). [b]This experiment used *cis-β*-IEPOX. All others used *trans-β*-IEPOX.
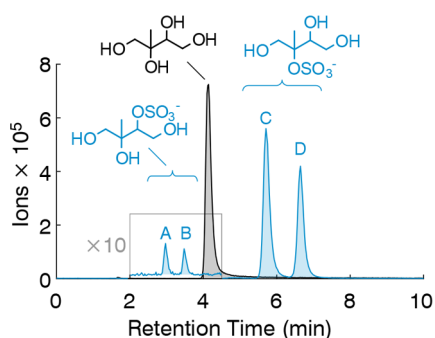

Figure 1. HILIC/(−)ESI-HR-QTOFMS extracted ion chromatograms (EICs) of authentic standards of 2-MTs (deprotonated ion, EIC *m/z* 135.066, black) and MTSs (deprotonated ion EIC, *m/z* 215.023, blue). MTS isomers 1,3,4-trihydroxy-3-methylbutan-2-yl sulfates (peaks A and B, RT 3.0 and 3.5 min, respectively) and 1,3,4-trihydroxy-2-methylbutan-2-yl sulfates (peaks C and D, RT 5.7 and 6.6 min, respectively). The HILIC conditions in this study do not resolve the 2-MT diastereomers 2-methylthreitol and 2-methylerythritol.

1,3,4-trihydroxy-3-methylbutan-2-yl sulfate).[31] Note that by the numbering convention applied to the IEPOX products, the isomers generated from *δ*-IEPOX + SO_4^{2-} are also 3-MTSs.[31,73] Quantification of MTS formation for kinetic analysis was accomplished by summing all EIC peak areas.

3. REACTION MECHANISM AND KINETICS

3.1. Mechanism. Schemes 1 and S1 show the acid-catalyzed epoxide ring-opening reaction of *trans-β*-IEPOX by three possible mechanisms to produce MTSs and 2-MTs. Acid-catalyzed mechanism A-1 is analogous to a unimolecular nucleophilic substitution reaction (S_N1) and involves a highly reactive carbocation intermediate (Scheme 1, top row). Acid-catalyzed mechanism A-2 is analogous to a bimolecular nucleophilic substitution reaction (S_N2) and is concerted (Scheme 1, middle row). These are both regarded as specific acid catalysis substitutions when the protonated solvent H_3O^+ is the catalyst. General acid catalysis occurs when an undissociated acid transfers a proton to the unprotonated epoxide oxygen during the rate-determining step (Scheme 1, bottom row).[91−94] Additional reactions (not pictured) occur between IEPOX and ammonium,[95] in aqueous pH-independ-

ent neutral reactions[93,95−99] following an A-2 mechanism,[93,99] and in base-catalyzed reactions.[93,95−99]

For acid-catalyzed ring opening to occur via A-1 or A-2 mechanisms, the epoxide must first be protonated in equilibrium with its conjugate base.[93,100,101] This pre-equilibrium protonation step has been demonstrated using isotopic rate ratios for various specific-acid catalyzed reactions,[99,101] including ring-opening of hydroxy-substituted epoxides similar to *β*-IEPOX.[52] The pK_a of the protonated conjugate acid of an epoxide has been estimated to be −2.8 for oxirane using density functional theory.[102] By comparison, the pK_a's of unstrained, acyclic protonated ethers, dimethyl ether and diethyl ether, are −2.48 and −2.39, respectively.[103]

3.2. Reaction Kinetics. The reaction rate was quantified as the disappearance of IEPOX over time assuming that all IEPOX is converted to either MTSs or 2-MTs. Note that MTSs and 2-MTs are the only expected products under the dilute conditions of this study.[10,31,104] Sulfate is not depleted appreciably during the reaction. Isomeric MTS dimers (*m/z* 333.086) and 2-MT dimers (*m/z* 253.129) have been detected in experiments conducted under concentrated conditions[31] but were below detection limits in this study. The rate law is thus represented as a pseudo-first order reaction:[74,105]

$$[\text{IEPOX}] \xrightarrow{k_{obs}} [\text{2-MTs}] + [\text{MTSs}] \tag{1a}$$

$$\frac{d[\text{IEPOX}]}{dt} = -k_{obs}[\text{IEPOX}] \tag{1b}$$

$$[\text{IEPOX}] \approx [\text{IEPOX}]_0 - [\text{2-MTs}] - [\text{MTSs}] \tag{1c}$$

Because ring opening is the rate-limiting step, this is the measured rate of product formation. Integration of eq 1b yields the rate equation,

$$\ln\left(\frac{[\text{IEPOX}]}{[\text{IEPOX}_0]}\right) = -k_{obs}t \tag{2}$$

The observed rate constant k_{obs} (s^{-1}) is the sum of all reaction rates breaking the epoxide C−O bond:[52,55,92,94,95]
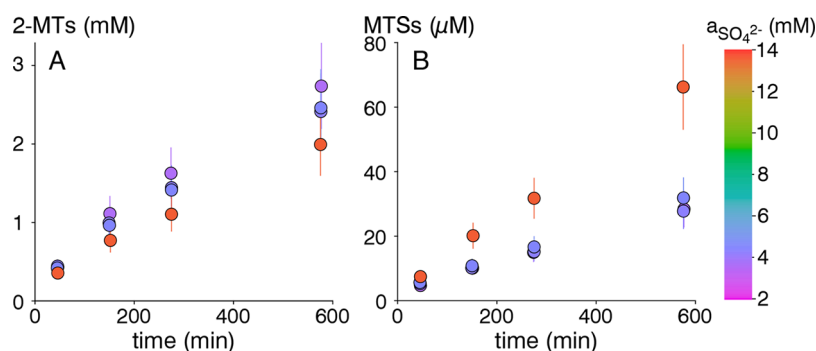
Figure 2. Growth in 2-methyltetrols (2-MTs) (A) and methyltetrol sulfates (MTSs) (B) during experiments with 5 mM *trans-β*-IEPOX varying sulfate (experiments #9−12 in Table 1).

$$k_{obs} = k^{A-1}a_{H^+} + k^{A-2}_{SO_4^{2-}}a_{SO_4^{2-}}a_{H^+} + k^{A-2}_{H_2O}a_{H_2O}a_{H^+}$$
$$+ k^{ga}_{HSO_4^-,SO_4^{2-}}a_{SO_4^{2-}}a_{HSO_4^-} + k^{ga}_{HSO_4^-,H_2O}a_{H_2O}a_{HSO_4^-}$$
$$+ k_{NH_4^+}a_{NH_4^+} + k_N \qquad (3)$$

Each rate coefficient k implicitly incorporates activity coefficients and standard state concentration units or the pK_a of the protonated epoxide as applicable. A detailed derivation is provided in the Supporting Information. Activity of species x in solution is denoted a_x, equivalent to $\gamma_x[x]/c^\ominus$, where γ_x is the unitless activity coefficient, $[x]$ is concentration, and $c^\ominus$ is the standard state concentration unit.[106] Because activities are used here, all coefficients have units of s^{-1} regardless of the rate order. The first term quantifies the spontaneous ring opening of the protonated epoxide to produce a carbocation intermediate via the A-1 mechanism. The second and third terms quantify the nucleophilic attack of the protonated epoxide via an A-2 mechanism. The a_{H^+} dependence of these first three terms is due to the a_{H^+} dependence of the protonated epoxide. The fourth and fifth terms quantify the third-order reaction of a general acid (bisulfate) protonating the epoxide in concert with nucleophilic attack. The last two terms quantify the depletion of IEPOX by hydrogen bond catalysis involving ammonia[95] and by the pH-independent neutral reaction with water.[95] The activities of all reactants depend on shifting solution equilibria. Thus, although only the A-1 and A-2 rate expressions depend explicitly on a_{H^+}, the general acid reaction rate is also affected by pH.

Table S3 compares estimated reaction rates for solutions considered in this work with published rates.[52,95,96,107] Because the rate with respect to H$_3$O$^+$ is at least an order of magnitude faster than the other ions, we can approximate k_{H^+} (M^{-1} s^{-1}) for the comparison and neglect other ions:

$$k_{H^+} = k_{obs}/(a_{H^+}c^\ominus) \qquad (4)$$

3.3. Product Branching Ratio. The branching ratio between 2-MTs and MTSs is defined as the molar ratio, β:

$$\beta = \frac{[MTSs]}{[2\text{-}MTs] + [MTSs]} \qquad (5)$$

The value of β depends on the concentrations of nucleophiles in solution and on the rate constants shown in eq 3. The branching ratio is defined such that the observed rates d[MTS]/dt and d[2-MT]/dt are equal to βk_{obs}[IEPOX] and $(1 − \beta)k_{obs}$[IEPOX], respectively.

3.4. Stereoisomers and Regioisomeric Enhancement. *Stereoisomers. trans-β*-IEPOX has two asymmetric carbons at which the nucleophile can add to the carbon backbone. Four MTS diastereomers (two at C2 and two at C3) can be formed from each *trans-β*-IEPOX enantiomer (Scheme 1, products **1−4**); thus racemic *trans-β*-IEPOX can yield a total of eight stereoisomers (Figure S1). 2-MT formation from *β*-IEPOX + H$_2$O yields two diastereomers, 2-methylthreitol and 2-methylerythritol (Products **5** and **6**; Scheme S1), each with enantiomers (denoted **a** and **b**), for a total of four isomers (Figure S2).[29] The HILIC/ESI-HR-QTOFMS method used in this work can resolve the diastereomers of MTSs (Figure 1 and section 2.3).[31]

Regioisomeric Selectivity. If substitution at one of the epoxide carbons is favored, the corresponding substitution product forms in excess. Products **1−2** in Scheme 1 represent substitution at C2, while **3−4** have been substituted at C3. Regioisomeric selectivity is then defined by[29]

$$re = \frac{[\text{tertiary MTSs}] − [\text{secondary MTSs}]}{[\text{tertiary MTSs}] + [\text{secondary MTSs}]} \times 100\% \qquad (6)$$

where [tertiary MTSs] is the sum of all tertiary MTS (Figure 1, peaks C and D), and [secondary MTSs] is the sum of all secondary MTSs (Figure 1, peaks A and B). In this work the peak areas of the EICs are taken as the relative quantities MTS isomers. The quantification is subject to error if the ionization efficiency differs significantly between tertiary and secondary isomers. Prior work shows that the ionization efficiency of MTS isomers derived from *β*-IEPOX is 1.23−1.78 times higher than the ionization efficiency of the 3-MTS diastereomers formed from substitution at the primary C of *δ*-IEPOX.[31] Factors influencing ionization efficiency include molecular structure and the mobile phase in the column, which changes in water content by up to 5% between retention times of the isomers. On the basis of the data reported for the major 3-MTS product from *δ*-IEPOX, differences in ionization efficiency between isomers compared in this work are likely less than a factor of 2. Given that the value of [secondary MTSs] is much less than [tertiary MTSs], a factor of 2 difference in ionization efficiency has a negligible impact on the value of *re*; thus, trends in *re* indicate changing experimental conditions, but absolute values of *re* cannot be compared between studies. Fractionation for NMR analysis of the isomeric structures was not feasible using this chromatography method. The specific MTS diastereomer associated with each chromatographic peak is discussed below.

4. RESULTS AND DISCUSSION

4.1. Reaction Kinetics. Figure 2 shows the formation of 2-MTs and MTSs during experiments as a function of varying sulfate concentration. In these experiments, 5 mM *trans-β*-IEPOX was reacted with 7−50 mM of total added sulfate at a target pH of 3, mimicking fog or polluted cloudwater conditions (lower sulfate) or concentrated fog droplets (50 mM added sulfate). Measured pH varied from 3.10 to 3.58. The 2-MT concentrations are significantly higher than the MTS concentrations because of the high water-to-sulfate ratios used in the dilute aqueous solutions. Note that the total added sulfate for lower sulfate concentration experiments is between 6.67 and 10 mM, about five times lower than in the high sulfate concentration experiment. Additional sulfate resulted in suppression of 2-MT formations relative to MTSs. Figure S3 shows the formation of 2-MTs and MTSs during experiments with varying pH and 5 mM of *trans-β*-IEPOX. Increased scatter is likely due to the high sensitivity to pH gradients within the mixture or at the air−water interface; this scatter was not reduced in repeated experiments nor by stirring the solutions. Under dilute conditions, a higher sulfate concentration is apparently helpful in buffering pH. Measured pH varied between 1.83 and 3.22. Reactions proceeded faster at lower pH as expected,[52,107] and 2-MT concentrations were generally ~100 times higher than the MTS concentrations due to the enhanced ratio of water-to-sulfate available to serve as a nucleophile in the epoxide ring-opening reaction. The *cis-β*-IEPOX experiment (#13 in Table 1) is included to show the chromatographic evidence for stereoisomeric products, which will be discussed below. One high-pH experiment (pH 5.02) was conducted with double the IEPOX concentration and only 0.3 mM of sulfate. This experiment demonstrated only that the reaction rate at this pH is too slow to quantify under the conditions of our experiments.

Table 3 and Figure S4 show the kinetic analysis for *trans-β*-IEPOX experiments. The effective rate constant k_{obs} is

Table 3. Observed Rate Coefficients and Branching Ratios

#	pH	k_{obs} ($\times 10^{-5}$ s^{-1})[a]	k_{H+} ($\times 10^{-2}$ M^{-1} s^{-1})[b]	β ($\times 10^{-2}$ mol mol^{-1})	std $\beta \times 10^2$
1	1.83	5.77	0.39	1.06	0.10
2	2.32	3.01	0.63	1.14	0.13
3	2.25	4.77	0.85	1.33	0.20
4	2.55	2.94	1.04	1.19	0.35
5	3.16	1.33	1.92	0.42	0.03
6	3.22	0.79	1.31	0.99	0.84
7	3.16	0.64	0.92	1.77	0.29
8	3.00	1.27	1.27	0.96	0.29
9	3.10	2.22	2.79	1.30	0.13
10	3.13	1.79	2.41	1.57	0.22
11	3.17	1.86	2.75	1.72	0.20
12	3.38	1.43	3.42	4.21	0.39
13[c]	2.79	1.20	0.74	0.87	0.71

^{a}From eq 2, $\ln\left(\frac{[\text{IEPOX}]}{[\text{IEPOX}_0]}\right) = -k_{obs}t$. ^{b}From eq 4, $k_{H+} = k_{obs}/(a_{H+}c^{\ominus})$.
^{c}This experiment used *cis-β*-IEPOX. All others used *trans-β*-IEPOX.

calculated as the (negative) slope of the linear fit to $\ln(\text{IEPOX}/\text{IEPOX}_0)$ vs time (eq 2) and ranged from 0.64 to 5.77×10^{-5} s^{-1} (varying pH with 5 mM *trans-β*-IEPOX) and from 1.42 to 2.22×10^{-5} s^{-1} (varying sulfate with 5 mM *trans-β*-IEPOX).

Figure 3 shows that the observed value of k_{H+} (eq 4 and Table 3) is comparable to published values derived from observations and structure−activity relationships based on more concentrated acidic solutions. The figure demonstrates that k_{H+} obtained in this work under the most dilute cloud- and fog-relevant conditions is lower than published values by up to an order of magnitude (panel A); agreement increases as the sulfate concentration is raised from fog-relevant (5−10 mM total sulfate) to polluted fog or aerosol-relevant values (50 mM total sulfate) (panel B). Because the rate limiting step in the A-1 mechanism is the spontaneous (unimolecular) epoxide ring opening, the sulfate dependence of k_{H+} demonstrated in Figure 3B supports the conclusion that the reaction is, at least in part, via an A-2 mechanism. Some studies represented in Figure 3 used sulfuric acid solutions but, due to the complexity of the solution, did not account for sulfate in the calculation of k_{H+} (as in this work and references M[74] and C[107] in Figure 3). Sulfate is known to participate in the epoxide ring-opening reaction through nucleophilic attack.[52,104] However, sulfate exerts a considerably weaker influence on epoxide ring-opening than H_3O^+ (see Table S3). This is not necessarily a reflection of the relative importance of A-1 versus A-2 ring opening—the overall rate expression includes H_3O^+ as a reactant in either case (due to the requisite pre-equilibrium protonation) (Scheme S5 and eqs 3, S2g, S3f, and S4f). In Figure 3A, we display the original model of Cole-Filipiak et al.[107] (solid black line) relative to published k_{H+} values. The dotted black line is our fit including additional studies not included in the original. Compare these first two models to a linear fit to all studies in which sulfate was either absent or accounted for in the derivation of k_{H+} (solid blue line). The comparison highlights that there is some variability in reported values of k_{H+} and that strong nucleophiles like sulfate likely introduce bias in these values. In the atmosphere, the abundance of other inorganic ions and of organic acids, some of which are themselves the products of isoprene oxidation,[8,108] will further perturb the observed reaction rate.

4.2. Branching Ratio. Figure 4 shows the branching ratio, β, between 2-MTs and MTSs for experiments with 5 mM *trans-β*-IEPOX and varying sulfate concentrations (experiments #9−12). Hydrolysis of MTS to form 2-MT is too slow to affect the branching ratio in this work.[80] Branching ratios obtained experimentally by Eddingsaas et al.[52] for *cis*-2,3-epoxybutane-1,4-diol, taken as the yield of the sulfate ester, are included for comparison and were higher than this work by a factor of four to five. This enhancement at a similar sulfate concentration could be due to the different epoxide used (a difference of one methyl group on C2).

The branching ratio obtained by Piletic et al.[102] for *β*-IEPOX using density functional theory is shown as a solid line. This branching ratio is obtained by comparing the rate expression for A-2 acid-catalyzed ring opening with sulfate as the nucleophile to the rate expression with water as the nucleophile ($k_{SO_4^{2-}}^{A-2} = 5.2 \times 10^{-1}$ M^{-2} s^{-1}, $k_{H_2O}^{A-2} = 5.3 \times 10^{-2}$ M^{-2} s^{-1}, and $[H_2O] = 55.5$ M):[102]

$$[\text{MTSs}] = k_{SO_4^{2-}}^{A-2}[\text{IEPOX}]a_{H+}a_{SO_4^{2-}}c^{\ominus 2}\Delta t \tag{7a}$$

$$[\text{2-MTs}] = k_{H_2O}^{A-2}[\text{IEPOX}]a_{H+}c^{\ominus}[H_2O]\Delta t \tag{7b}$$

Substitution of eqs 7a and 7b in eq 5 explains why the branching ratio β varies with $a_{SO_4^{2-}}$ in this calculation and is independent of pH.
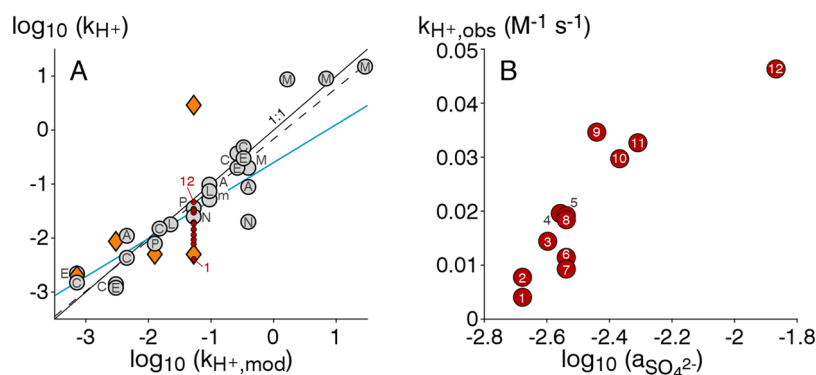
Figure 3. (A) Comparison of k_{H+} to the regression model of Cole-Filipiak et al.[107] ($k_{H+,mod}$). Gray circles: published observations (letters denote sources: M,[74] C,[107] E,[52] A,[104] L,[97] P,[9] m,[96] and N[95]). Solid black line: 1:1 line (equal to original regression model, which incorporated observations of M, C, L and P).[107] Dotted black line: fit to all published observations including those of E, A, m, and N, added here as an extension of the original. Solid blue line: fit to all studies except M, C, and this work, which ignore sulfate in calculation of k_{H+}. Orange diamonds: k_{H+} estimated from structure−activity relationships by Eddingsaas[52] and DFT simulations of Piletic[102] and co-workers. Red circles: observed k_{H+}, this work (*trans-β*-IEPOX). Red numbers: experiment number in Table 3. (B) Observed of k_{H+}, this work, as a function of sulfate ion activity (mol L^{−1} basis) (*trans-β*-IEPOX; derived via eq 4). Numbers: experiment number in Table 3.
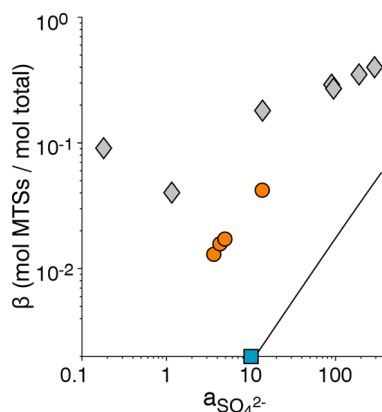

Figure 4. Branching ratio, β, for experiments #9−12 varying sulfate ion activity (mmol L^{−1} basis) (red circles). Diamonds: Eddingsaas et al.[52] for *cis*-2,3-epoxybutane-1,4-diol; Line: Piletic et al.[102] Blue square: branching ratio calculated using relative nucleophilic strengths of sulfate and H_2O.[109]

Branching ratios observed under cloud-relevant conditions are significantly lower than those obtained for deliquescent aerosols due to the relative scarcity of the sulfate ion available as a nucleophile in the ring-opening reaction of these epoxides. The sulfate concentration in these experiments is closer to that of a fog than to cloudwater, where total sulfate can range from 0.06 to 0.1 mM,[87] meaning that the branching ratio in cloudwater is likely lower than shown in Figure 4 by at least a factor of 10. Past estimates have branching ratios of ~0.4,[50,52] likely overpredicting in-cloud MTS formation. Likewise, because most IEPOX reacting in cloudwater will result in 2-MTs and not in MTSs, using sole measurements of MTS isomers to track in-cloud reactions of IEPOX may significantly underestimate the dark reactions of IEPOX in cloudwater.

The branching ratio between 2-MTs and MTSs is low; it is nevertheless much higher than the ratio calculated on the basis of the competitive A-1 mechanism, which would result in a branching ratio calculated solely on the basis of relative nucleophilic strengths of sulfate and H_2O (estimated as ~11-fold)[109] and relative concentrations (β ~2 × 10^{−3} for a 10 mM sulfate solution). The experimentally derived data for β therefore provides support for an A-2-like mechanism.

Interestingly, the branching ratio calculated based on A-1 seems to be close to the curve of Piletic et al.[102] in Figure 4.

4.3. Identification of Stereoisomers and Mechanism.
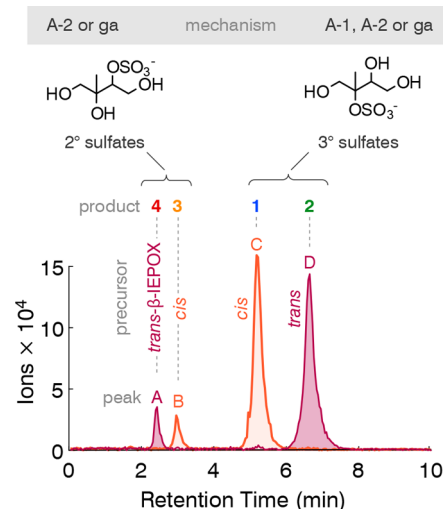Figure 5 compares the EICs of the MTS isomers that form

Figure 5. HILIC/(−)ESI-HR-QTOFMS EICs of the four MTS isomers detected from *trans-β*-IEPOX (pink EIC, peaks A and D) and *cis-β*-IEPOX (orange EIC, peaks B and C). Hypothesized products, product properties, and reaction mechanisms are noted above peaks.

during the reaction of *trans-β*-IEPOX (peaks A and D, experiment #5) and *cis-β*-IEPOX (peaks B and C, experiment #13). The target of the synthetic route to the MTS standard was the mixture of 2-MTS diastereomers, and a minor amount of the secondary 3-MTS diastereomers was produced as byproducts. In the chromatogram of the standard (Figure 1, section 2.3), the 2-MTS diastereomers elute as peaks C and D. By default, we attribute peaks A and B to the diastereomers from substitution at the secondary carbon, as shown in Scheme 1. Differentiation between diastereomers was not possible using MS/MS. A striking feature of Figure 5 is that sulfation of *trans-* and *cis-β*-IEPOX each yields almost exclusively a single diastereomer of both major and minor sulfate esters.
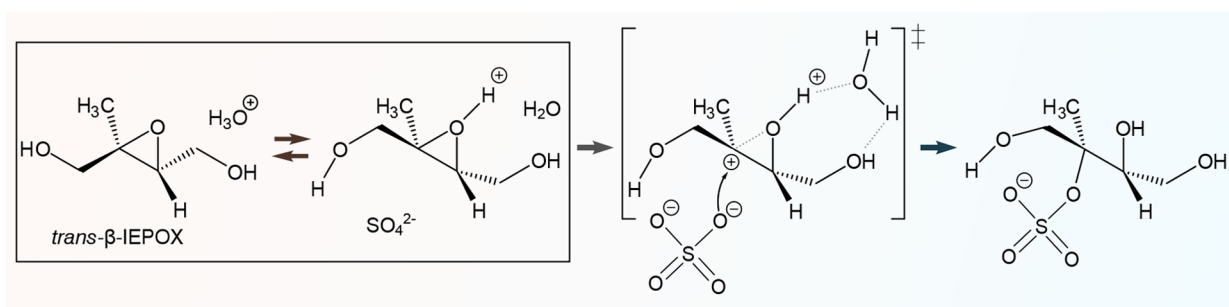
Figure 6. Transition state proposed for nucleophilic attack on protonated *trans-β*-IEPOX leading to the major observed isomer.
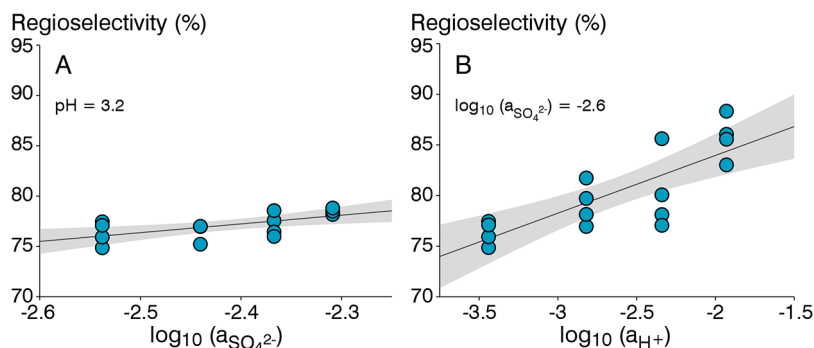

Figure 7. Regioselectivity of tertiary sulfate under varying SO_4^{2-} activity (A) and varying H_3O^+ activity (B), following eq 6 (section 3.4). The linear best fit and 95% confidence interval of the slope are shown. Activities correspond to mol L^{-1}.

Substitutions are generally described in terms of A-1 and the A-2 mechanisms. Past studies have used isotopic rate ratios to shed light on the mechanism,[52] but the *β*-IEPOX reaction remains ambiguous by this method.[93,100,102] Other studies have also drawn mixed conclusions regarding tertiary MTS products.[31,52,74,102] A-1 and A-2 substitutions at asymmetric centers can be distinguished by the distribution of stereo-isomers formed in the reaction, with inversion of optical configuration occurring for A-2 and epimerization for A-1. To the extent that both mechanisms are operative, there will be a greater or lesser excess of one enantiomeric product. In the case of *trans-* and *cis-β*-IEPOX, the presence of adjacent asymmetric centers at C2 and C3 results in resolvable diastereomeric products. Thus, epimerization at C2 or C3 via an A-1 mechanism will result in the simultaneous presence of all four diastereomers in the products of *trans-β*-IEPOX or *cis-β*-IEPOX. As Figure 5 indicates, there is virtually no epimerization at either asymmetric center.

The mechanism of substitution as well as regioselectivity for substitution at C2 appears to be nuanced, and definitive arguments are precluded by the fact that the absolute stereochemistry of the products cannot be assigned at this time. As a rule, the A-1 mechanism is favored by highly stabilized carbocation intermediates. While the electron donating C2 methyl group of *β*-IEPOX can stabilize a developing positive charge, this effect is mitigated by the C1 hydroxymethyl substituent, which might be expected to exert a destabilizing electron-withdrawing effect. The *β*-hydroxy group of a carbonium is also stabilizing;[110] however, both C2 and C3 are equally subject to this effect. The stabilizing effect of an electron releasing substituent at C3 is absent. Overall, a carbonium ion at either C2 or C3 would not seem highly stabilized, and an A-1 mechanism does not seem favorable at either carbon. Based only on electronic effects, substitution at

C2 is favored.[93] While steric effects usually favor substitution at less hindered sites (C3 in the case of *trans-* and *cis-β*-IEPOX), this effect is expected to be less critical for the oxirane structure in comparison to a normal acyclic substrate. Theoretical treatment of *trans-β*-IEPOX predicts substitution at C2,[102] consistent with our experimental observations, supporting the importance of electronic considerations. The *α*-hydroxy oxirane structural motif may shed light on the stereochemistry as illustrated in Figure 6. The C1 OH can interact with the incipient C2 carbonium ion in the transition state, which is similar to that of an acid-catalyzed Payne rearrangement,[111] and the C4 hydroxy substituent can interact with the oxirane oxygen through hydrogen bonds with or without an intervening water molecule. This transition state could direct the approach of sulfate and result in predominance of either retention or inversion of optical configuration at C2. Since absolute stereochemistry cannot be assigned at this time, a more specific description of the substitution cannot be postulated. A similar mechanism could be in play at C3.

4.4. Effect of Reaction Environment on Regioselectivity of Sulfate Addition. Figure 7 illustrates the enhancement of the tertiary MTSs (peaks C and D) over the secondary isomers (peaks A and B) as a function of SO_4^{2-} or H_3O^+ activity or pH. Increasing the sulfate concentration marginally increases the tertiary isomer, whereas lowering pH (increasing H_3O^+ activity) markedly enhances the tertiary isomer. Stabilization of the transition state by the C2-methyl substituent and participation of the C1 hydroxy group (Figure 6) during scission of the C2−O epoxide bond can account for the selectivity for substitution at C2. Decreased selectivity of substitution at C2 with decreasing pH may be a function of stabilization of the unprotonated oxirane by the C1 hydroxy group, causing the bulky methyl group to block the approach of sulfate toward the tertiary C2 in a textbook case of steric

hindrance. The experiments shown were performed and analyzed in concert; additional experiments were elided due to the sensitivity of the analytical method to subtle changes in operation conditions on different days (see section 3.4).

In conclusion, Figures 5 and 6 provide insights into a plausible mechanism for oxirane ring opening of *trans*-*β*-IEPOX, the major product of atmospheric photochemical oxidation of isoprene,[26] and could prove helpful in understanding the processing of IEPOX to isomeric MTSs over the broad pH ranges observed in aerosols, fogs, and cloud droplets.

5. SUMMARY AND ATMOSPHERIC IMPLICATIONS

An experimental investigation of the reaction of *trans*-*β*-IEPOX under fog- and cloud-relevant conditions, varying either pH or total sulfate, is presented. Comparisons are made with *cis*-*β*-IEPOX. The reaction rate in cloudwater is slower than in deliquescent aerosols due to the higher pH and more dilute conditions. Note that due to the high water content in clouds and fogs and the high Henry's Law constant of IEPOX, the contribution of cloud and fogwater reactions to IEPOX SOA may still exceed that of aerosol reactions under some circumstances (e.g., pH < ~4).[50] Also, additional reactions could occur during droplet evaporation,[49,112,113] which was not studied here. The rate constant for the acid-catalyzed ring-opening reaction, k_{H+}, is comparable to predicted k_{H+} using structure−activity relationships reported by other authors;[52,102,107] however, the strong dependence of observed rate constant k_{H+} on the activity of the sulfate ion indicates that sulfate activity contributes to k_{H+}. Our k_{H+} value observed at low sulfate concentrations ($3.9-6.3 \times 10^{-3}$ M^{-1} s^{-1}) is likely closer to the value expected for purely acid-catalyzed reactions omitting the influence of other nucleophiles in solution. In cloudwater, participation of weak acids such as acetic, formic, or oxalic acid could enhance reaction rates through concerted protonation by an undissociated acid and addition of a nucleophile.

The branching ratio between MTS and 2-MT products of IEPOX reaction in acidified sulfate varied between 0.013 and 0.042 at constant pH ≈ 3 with total sulfate between 5 and 50 mM, 2 orders of magnitude lower than previous experimental results using highly concentrated sulfate solutions (>1 M total sulfate[9,52,74,107]). Dimers or higher oligomers of 2-MTs or MTSs were not observed under our experimental conditions. The strong dependence of branching ratio on sulfate activity shows that under cloud-relevant conditions, the reaction of dissolved IEPOX will predominantly result in the formation of 2-MTs. Observational studies tracking in-cloud chemistry could substantially underestimate the aqueous reactions of *cis*- and *trans*-*β*-IEPOX if MTS products are used exclusively as a tracer.

Stereoisomers of MTS from *trans*- and *cis*-*β*-IEPOX reveal that the acid-catalyzed reaction likely involves participation of neighboring substituents in a ring-opening mechanism having A-2 characteristics, predominantly at the tertiary carbon. Evidence from varying secondary-to-tertiary MTS product ratios indicates that pH exerts a control on the mechanistic pathway, pushing the reaction toward the tertiary isomers at lower pH. Varying sulfate had minimal impact on the distribution of MTS isomers. These observations indicate that atmospheric conditions could control isomeric product distributions and thus the physical properties and reactivities of the product resulting mixtures. As such, the stereochemical distribution holds promise as a tracer for the relative

contributions of organosulfate formation under differing atmospheric conditions (e.g., cloud conditions vs aerosol conditions) as has been done for isoprene-derived tetrols[29,75] and for pollutant degradation.[114] Uncertainties in the equilibria between ions in solution contribute to uncertainties in the mechanism. Further research is needed to better understand the effect of organic/inorganic mixing on reaction rates and stereochemistry. Nevertheless, the process-level insight into the mechanistic controls on observed rate constants, branching ratios, and stereoisomers will likely be helpful in making predictions of IEPOX reactions under atmospheric conditions such as those of cloud or fog droplets.

■ ASSOCIATED CONTENT

🅂🅸 Supporting Information
The Supporting Information is available free of charge at https://pubs.acs.org/doi/10.1021/acsearthspace-chem.0c00293.

Four figures, five schemes, and three tables (PDF)

■ AUTHOR INFORMATION

Corresponding Author
Sarah S. Petters − *Department of Environmental Sciences and Engineering, Gillings School of Global Public Health, The University of North Carolina at Chapel Hill, Chapel Hill, North Carolina 27599, United States;* ◎ orcid.org/0000-0002-4501-7127; Email: spetters@unc.edu

Authors
Tianqu Cui − *Department of Environmental Sciences and Engineering, Gillings School of Global Public Health, The University of North Carolina at Chapel Hill, Chapel Hill, North Carolina 27599, United States*

Zhenfa Zhang − *Department of Environmental Sciences and Engineering, Gillings School of Global Public Health, The University of North Carolina at Chapel Hill, Chapel Hill, North Carolina 27599, United States*

Avram Gold − *Department of Environmental Sciences and Engineering, Gillings School of Global Public Health, The University of North Carolina at Chapel Hill, Chapel Hill, North Carolina 27599, United States*

V. Faye McNeill − *Departments of Chemical Engineering and Earth and Environmental Sciences, Columbia University, New York 10027, United States;* ◎ orcid.org/0000-0003-0379-6916

Jason D. Surratt − *Department of Environmental Sciences and Engineering, Gillings School of Global Public Health and Department of Chemistry, The University of North Carolina at Chapel Hill, Chapel Hill, North Carolina 27599, United States;* ◎ orcid.org/0000-0002-6833-1450

Barbara J. Turpin − *Department of Environmental Sciences and Engineering, Gillings School of Global Public Health, The University of North Carolina at Chapel Hill, Chapel Hill, North Carolina 27599, United States*

Complete contact information is available at:
https://pubs.acs.org/10.1021/acsearthspacechem.0c00293

■ REFERENCES

(1) IPCC, 2013: Summary for Policymakers. In *Climate Change 2013: The Physical Science Basis. Contribution of Working Group I to the Fifth Assessment Report of the Intergovernmental Panel on Climate Change*; Stocker, T. F., Qin, D., Plattner, G.-K., Tignor, M., Allen, S. K., Boschung, J., Nauels, A., Xia, Y., Bex, V.; Midgley, P. M., Eds.; Cambridge University Press: Cambridge, United Kingdom and New York, NY, USA, 2013.

(2) Kreidenweis, S. M.; Petters, M.; Lohmann, U. 100 Years of Progress in Cloud Physics, Aerosols, and Aerosol Chemistry Research. *Meteorol. Monogr.* **2019**, *59*, 11.1−11.72.

(3) Apte, J. S.; Marshall, J. D.; Cohen, A. J.; Brauer, M. Addressing Global Mortality from Ambient PM2. *Environ. Sci. Technol.* **2015**, *49* (13), 8057−8066.

(4) West, J. J.; Cohen, A.; Dentener, F.; Brunekreef, B.; Zhu, T.; Armstrong, B.; Bell, M. L.; Brauer, M.; Carmichael, G.; Costa, D. L.; Dockery, D. W.; Kleeman, M.; Krzyzanowski, M.; Künzli, N.; Liousse, C.; Lung, S.-C. C.; Martin, R. V.; Pöschl, U.; Pope, C. A.; Roberts, J. M.; Russell, A. G.; Wiedinmyer, C. What We Breathe Impacts Our Health: Improving Understanding of the Link between Air Pollution and Health. *Environ. Sci. Technol.* **2016**, *50* (10), 4895−4904.

(5) Zhang, Q.; Jimenez, J. L.; Canagaratna, M. R.; Allan, J. D.; Coe, H.; Ulbrich, I.; Alfarra, M. R.; Takami, A.; Middlebrook, A. M.; Sun, Y. L.; Dzepina, K.; Dunlea, E. J.; Docherty, K. S.; DeCarlo, P. F.; Salcedo, D.; Onasch, T.; Jayne, J. T.; Miyoshi, T.; Shimono, A.; Hatakeyama, S.; Takegawa, N.; Kondo, Y.; Schneider, J.; Drewnick, F.; Borrmann, S.; Weimer, S.; Demerjian, K.; Williams, P.; Bower, K.; Bahreini, R.; Cottrell, L.; Griffin, R. J.; Rautiainen, J.; Sun, J. Y.; Zhang, Y. M.; Worsnop, D. R. Ubiquity and Dominance of Oxygenated Species in Organic Aerosols in Anthropogenically-Influenced Northern Hemisphere Midlatitudes. *Geophys. Res. Lett.* **2007**, *34* (13), L13801.

(6) Guenther, A. B.; Jiang, X.; Heald, C. L.; Sakulyanontvittaya, T.; Duhl, T.; Emmons, L. K.; Wang, X. The Model of Emissions of Gases and Aerosols from Nature Version 2.1 (MEGAN2.1): An Extended and Updated Framework for Modeling Biogenic Emissions. *Geosci. Model Dev.* **2012**, *5* (6), 1471−1492.

(7) Arneth, A.; Schurgers, G.; Lathiere, J.; Duhl, T.; Beerling, D. J.; Hewitt, C. N.; Martin, M.; Guenther, A. Global Terrestrial Isoprene Emission Models: Sensitivity to Variability in Climate and Vegetation. *Atmos. Chem. Phys.* **2011**, *11* (15), 8037−8052.

(8) Wennberg, P. O.; Bates, K. H.; Crounse, J. D.; Dodson, L. G.; McVay, R. C.; Mertens, L. A.; Nguyen, T. B.; Praske, E.; Schwantes, R. H.; Smarte, M. D.; St Clair, J. M.; Teng, A. P.; Zhang, X.; Seinfeld, J. H. Gas-Phase Reactions of Isoprene and Its Major Oxidation Products. *Chem. Rev.* **2018**, *118* (7), 3337−3390.

(9) Paulot, F.; Crounse, J. D.; Kjaergaard, H. G.; Kürten, A.; St. Clair, J. M.; Seinfeld, J. H.; Wennberg, P. O. Unexpected Epoxide Formation in the Gas-Phase Photooxidation of Isoprene. *Science* **2009**, *325* (5941), 730−733.

(10) Surratt, J. D.; Chan, A. W. H.; Eddingsaas, N. C.; Chan, M.; Loza, C. L.; Kwan, A. J.; Hersey, S. P.; Flagan, R. C.; Wennberg, P. O.; Seinfeld, J. H. Reactive Intermediates Revealed in Secondary Organic Aerosol Formation from Isoprene. *Proc. Natl. Acad. Sci. U. S. A.* **2010**, *107* (15), 6640−6645.

(11) Riva, M.; Chen, Y.; Zhang, Y.; Lei, Z.; Olson, N. E.; Boyer, H. C.; Narayan, S.; Yee, L. D.; Green, H. S.; Cui, T.; Zhang, Z.; Baumann, K.; Fort, M.; Edgerton, E.; Budisulistiorini, S. H.; Rose, C. A.; Ribeiro, I. O.; e Oliveira, R. L.; dos Santos, E. O.; Machado, C. M.

D.; Szopa, S.; Zhao, Y.; Alves, E. G.; de Sá, S. S.; Hu, W.; Knipping, E. M.; Shaw, S. L.; Duvoisin Junior, S.; de Souza, R. A. F.; Palm, B. B.; Jimenez, J.-L.; Glasius, M.; Goldstein, A. H.; Pye, H. O. T.; Gold, A.; Turpin, B. J.; Vizuete, W.; Martin, S. T.; Thornton, J. A.; Dutcher, C. S.; Ault, A. P.; Surratt, J. D. Increasing Isoprene Epoxydiol-to-Inorganic Sulfate Aerosol Ratio Results in Extensive Conversion of Inorganic Sulfate to Organosulfur Forms: Implications for Aerosol Physicochemical Properties. *Environ. Sci. Technol.* **2019**, *53* (15), 8682−8694.

(12) Mao, J.; Carlton, A.; Cohen, R. C.; Brune, W. H.; Brown, S. S.; Wolfe, G. M.; Jimenez, J. L.; Pye, H. O. T.; Lee Ng, N.; Xu, L.; McNeill, V. F.; Tsigaridis, K.; McDonald, B. C.; Warneke, C.; Guenther, A.; Alvarado, M. J.; de Gouw, J.; Mickley, L. J.; Leibensperger, E. M.; Mathur, R.; Nolte, C. G.; Portmann, R. W.; Unger, N.; Tosca, M.; Horowitz, L. W. Southeast Atmosphere Studies: Learning from Model-Observation Syntheses. *Atmos. Chem. Phys.* **2018**, *18* (4), 2615−2651.

(13) Marais, E. A.; Jacob, D. J.; Jimenez, J. L.; Campuzano-Jost, P.; Day, D. A.; Hu, W.; Krechmer, J.; Zhu, L.; Kim, P. S.; Miller, C. C.; Fisher, J. A.; Travis, K.; Yu, K.; Hanisco, T. F.; Wolfe, G. M.; Arkinson, H. L.; Pye, H. O. T.; Froyd, K. D.; Liao, J.; McNeill, V. F. Aqueous-Phase Mechanism for Secondary Organic Aerosol Formation from Isoprene: Application to the Southeast United States and Co-Benefit of SO₂ Emission Controls. *Atmos. Chem. Phys.* **2016**, *16* (3), 1603−1618.

(14) Budisulistiorini, S. H.; Li, X.; Bairai, S. T.; Renfro, J.; Liu, Y.; Liu, Y. J.; McKinney, K. A.; Martin, S. T.; McNeill, V. F.; Pye, H. O. T.; Nenes, A.; Neff, M. E.; Stone, E. A.; Mueller, S.; Knote, C.; Shaw, S. L.; Zhang, Z.; Gold, A.; Surratt, J. D. Examining the Effects of Anthropogenic Emissions on Isoprene-Derived Secondary Organic Aerosol Formation during the 2013 Southern Oxidant and Aerosol Study (SOAS) at the Look Rock, Tennessee Ground Site. *Atmos. Chem. Phys.* **2015**, *15* (15), 8871−8888.

(15) Budisulistiorini, S. H.; Nenes, A.; Carlton, A. G.; Surratt, J. D.; McNeill, V. F.; Pye, H. O. T. Simulating Aqueous-Phase Isoprene-Epoxydiol (IEPOX) Secondary Organic Aerosol Production During the 2013 Southern Oxidant and Aerosol Study (SOAS). *Environ. Sci. Technol.* **2017**, *51* (9), 5026−5034.

(16) Hu, W. W.; Campuzano-Jost, P.; Palm, B. B.; Day, D. A.; Ortega, A. M.; Hayes, P. L.; Krechmer, J. E.; Chen, Q.; Kuwata, M.; Liu, Y. J.; de Sa, S. S.; McKinney, K.; Martin, S. T.; Hu, M.; Budisulistiorini, S. H.; Riva, M.; Surratt, J. D.; St. Clair, J. M.; Isaacman-Van Wertz, G.; Yee, L. D.; Goldstein, A. H.; Carbone, S.; Brito, J.; Artaxo, P.; de Gouw, J. A.; Koss, A.; Wisthaler, A.; Mikoviny, T.; Karl, T.; Kaser, L.; Jud, W.; Hansel, A.; Docherty, K. S.; Alexander, M. L.; Robinson, N. H.; Coe, H.; Allan, J. D.; Canagaratna, M. R.; Paulot, F.; Jimenez, J. L. Characterization of a Real-Time Tracer for Isoprene Epoxydiols-Derived Secondary Organic Aerosol (IEPOX-SOA) from Aerosol Mass Spectrometer Measurements. *Atmos. Chem. Phys.* **2015**, *15* (20), 11807−11833.

(17) Xu, L.; Guo, H.; Boyd, C. M.; Klein, M.; Bougiatioti, A.; Cerully, K. M.; Hite, J. R.; Isaacman-VanWertz, G.; Kreisberg, N. M.; Knote, C.; Olson, K.; Koss, A.; Goldstein, A. H.; Hering, S. V.; de Gouw, J.; Baumann, K.; Lee, S.-H.; Nenes, A.; Weber, R. J.; Ng, N. L. Effects of Anthropogenic Emissions on Aerosol Formation from Isoprene and Monoterpenes in the Southeastern United States. *Proc. Natl. Acad. Sci. U. S. A.* **2015**, *112* (1), 37.

(18) Budisulistiorini, S. H.; Canagaratna, M. R.; Croteau, P. L.; Marth, W. J.; Baumann, K.; Edgerton, E. S.; Shaw, S. L.; Knipping, E. M.; Worsnop, D. R.; Jayne, J. T.; Gold, A.; Surratt, J. D. Real-Time Continuous Characterization of Secondary Organic Aerosol Derived from Isoprene Epoxydiols in Downtown Atlanta, Georgia, Using the Aerodyne Aerosol Chemical Speciation Monitor. *Environ. Sci. Technol.* **2013**, *47* (11), 5686−5694.

(19) Budisulistiorini, S. H.; Baumann, K.; Edgerton, E. S.; Bairai, S. T.; Mueller, S.; Shaw, S. L.; Knipping, E. M.; Gold, A.; Surratt, J. D. Seasonal Characterization of Submicron Aerosol Chemical Composition and Organic Aerosol Sources in the Southeastern United States:

Atlanta, Georgia, and Look Rock, Tennessee. *Atmos. Chem. Phys.* **2016**, *16* (8), 5171−5189.

(20) Rattanavaraha, W.; Chu, K.; Budisulistiorini, S. H.; Riva, M.; Lin, Y.-H.; Edgerton, E. S.; Baumann, K.; Shaw, S. L.; Guo, H.; King, L.; Weber, R. J.; Neff, M. E.; Stone, E. A.; Offenberg, J. H.; Zhang, Z.; Gold, A.; Surratt, J. D. Assessing the Impact of Anthropogenic Pollution on Isoprene-Derived Secondary Organic Aerosol Formation in PM2.5 Collected from the Birmingham, Alabama, Ground Site during the 2013 Southern Oxidant and Aerosol Study. *Atmos. Chem. Phys.* **2016**, *16* (8), 4897−4914.

(21) Rattanavaraha, W.; Canagaratna, M. R.; Budisulistiorini, S. H.; Croteau, P. L.; Baumann, K.; Canonaco, F.; Prevot, A. S. H.; Edgerton, E. S.; Zhang, Z.; Jayne, J. T.; Worsnop, D. R.; Gold, A.; Shaw, S. L.; Surratt, J. D. Source Apportionment of Submicron Organic Aerosol Collected from Atlanta, Georgia, during 2014−2015 Using the Aerosol Chemical Speciation Monitor (ACSM). *Atmos. Environ.* **2017**, *167*, 389−402.

(22) Schulz, C.; Schneider, J.; Amorim Holanda, B.; Appel, O.; Costa, A.; de Sá, S. S.; Dreiling, V.; Fütterer, D.; Jurkat-Witschas, T.; Klimach, T.; Knote, C.; Krämer, M.; Martin, S. T.; Mertes, S.; Pöhlker, M. L.; Sauer, D.; Voigt, C.; Walser, A.; Weinzierl, B.; Ziereis, H.; Zöger, M.; Andreae, M. O.; Artaxo, P.; Machado, L. A. T.; Pöschl, U.; Wendisch, M.; Borrmann, S. Aircraft-Based Observations of Isoprene-Epoxydiol-Derived Secondary Organic Aerosol (IEPOX-SOA) in the Tropical Upper Troposphere over the Amazon Region. *Atmos. Chem. Phys.* **2018**, *18* (20), 14979−15001.

(23) de Sá, S. S.; Palm, B. B.; Campuzano-Jost, P.; Day, D. A.; Newburn, M. K.; Hu, W.; Isaacman-VanWertz, G.; Yee, L. D.; Thalman, R.; Brito, J.; Carbone, S.; Artaxo, P.; Goldstein, A. H.; Manzi, A. O.; Souza, R. A. F.; Mei, F.; Shilling, J. E.; Springston, S. R.; Wang, J.; Surratt, J. D.; Alexander, M. L.; Jimenez, J. L.; Martin, S. T. Influence of Urban Pollution on the Production of Organic Particulate Matter from Isoprene Epoxydiols in Central Amazonia. *Atmos. Chem. Phys.* **2017**, *17* (11), 6611−6629.

(24) Stadtler, S.; Kühn, T.; Schröder, S.; Taraborrelli, D.; Schultz, M. G.; Kokkola, H. Isoprene-Derived Secondary Organic Aerosol in the Global Aerosol−Chemistry−Climate Model ECHAM6.3.0−HAM2.3−MOZ1.0. *Geosci. Model Dev.* **2018**, *11* (8), 3235−3260.

(25) Froyd, K. D.; Murphy, S. M.; Murphy, D. M.; de Gouw, J. A.; Eddingsaas, N. C.; Wennberg, P. O. Contribution of Isoprene-Derived Organosulfates to Free Tropospheric Aerosol Mass. *Proc. Natl. Acad. Sci. U. S. A.* **2010**, *107* (50), 21360.

(26) Bates, K. H.; Crounse, J. D.; St. Clair, J. M.; Bennett, N. B.; Nguyen, T. B.; Seinfeld, J. H.; Stoltz, B. M.; Wennberg, P. O. Gas Phase Production and Loss of Isoprene Epoxydiols. *J. Phys. Chem. A* **2014**, *118* (7), 1237−1246.

(27) Kourtchev, I.; Ruuskanen, T.; Maenhaut, W.; Kulmala, M.; Claeys, M. Observation of 2-Methyltetrols and Related Photo-Oxidation Products of Isoprene in Boreal Forest Aerosols from Hyytiälä, Finland. *Atmos. Chem. Phys.* **2005**, *5* (10), 2761−2770.

(28) Ion, A. C.; Vermeylen, R.; Kourtchev, I.; Cafmeyer, J.; Chi, X.; Gelencsér, A.; Maenhaut, W.; Claeys, M. Polar Organic Compounds in Rural PM2.5 Aerosols from K-Puszta, Hungary, during a 2003 Summer Field Campaign: Sources and Diel Variations. *Atmos. Chem. Phys.* **2005**, *5* (7), 1805−1814.

(29) Nozière, B.; González, N. J. D.; Borg-Karlson, A.-K.; Pei, Y.; Redeby, J. P.; Krejci, R.; Dommen, J.; Prevot, A. S. H.; Anthonsen, T. Atmospheric Chemistry in Stereo: A New Look at Secondary Organic Aerosols from Isoprene. *Geophys. Res. Lett.* **2011**, *38* (11). DOI: 10.1029/2011GL047323.

(30) Claeys, M.; Graham, B.; Vas, G.; Wang, W.; Vermeylen, R.; Pashynska, V.; Cafmeyer, J.; Guyon, P.; Andreae, M. O.; Artaxo, P.; Maenhaut, W. Formation of Secondary Organic Aerosols through Photooxidation of Isoprene. *Science* **2004**, *303* (5661), 1173−1176.

(31) Cui, T.; Zeng, Z.; dos Santos, E. O.; Zhang, Z.; Chen, Y.; Zhang, Y.; Rose, C. A.; Budisulistiorini, S. H.; Collins, L. B.; Bodnar, W. M.; de Souza, R. A. F.; Martin, S. T.; Machado, C. M. D.; Turpin, B. J.; Gold, A.; Ault, A. P.; Surratt, J. D. Development of a Hydrophilic Interaction Liquid Chromatography (HILIC) Method for the

Chemical Characterization of Water-Soluble Isoprene Epoxydiol (IEPOX)-Derived Secondary Organic Aerosol. *Environ. Sci. Process. Impacts* **2018**, *20* (11), 1524−1536.

(32) Hettiyadura, A. P. S.; Al-Naiema, I. M.; Hughes, D. D.; Fang, T.; Stone, E. A. Organosulfates in Atlanta, Georgia: Anthropogenic Influences on Biogenic Secondary Organic Aerosol Formation. *Atmos. Chem. Phys.* **2019**, *19* (5), 3191−3206.

(33) Hughes, D. D.; Christiansen, M. B.; Milani, A.; Vermeuel, M. P.; Novak, G. A.; Alwe, H. D.; Dickens, A. F.; Pierce, R. B.; Millet, D. B.; Bertram, T. H.; Stanier, C. O.; Stone, E. A. PM2.5 Chemistry, Organosulfates, and Secondary Organic Aerosol during the 2017 Lake Michigan Ozone Study. *Atmos. Environ.* **2021**, *244*, 117939.

(34) Tolocka, M. P.; Turpin, B. Contribution of Organosulfur Compounds to Organic Aerosol Mass. *Environ. Sci. Technol.* **2012**, *46* (15), 7978−7983.

(35) Hoyle, C. R.; Boy, M.; Donahue, N. M.; Fry, J. L.; Glasius, M.; Guenther, A.; Hallar, A. G.; Huff Hartz, K. E.; Petters, M. D.; Petäjä, T.; Rosenoern, T.; Sullivan, A. P. A Review of the Anthropogenic Influence on Biogenic Secondary Organic Aerosol. *Atmos. Chem. Phys.* **2011**, *11* (1), 321−343.

(36) Liao, J.; Froyd, K. D.; Murphy, D. M.; Keutsch, F. N.; Yu, G.; Wennberg, P. O.; St. Clair, J. M.; Crounse, J. D.; Wisthaler, A.; Mikoviny, T.; Jimenez, J. L.; Campuzano-Jost, P.; Day, D. A.; Hu, W.; Ryerson, T. B.; Pollack, I. B.; Peischl, J.; Anderson, B. E.; Ziemba, L. D.; Blake, D. R.; Meinardi, S.; Diskin, G. Airborne Measurements of Organosulfates over the Continental U.S. *J. Geophys. Res.: Atmos.* **2015**, *120* (7), 2990−3005.

(37) Atkinson, R.; Arey, J. Atmospheric Degradation of Volatile Organic Compounds. *Chem. Rev.* **2003**, *103* (12), 4605−4638.

(38) Liu, Y.; Seco, R.; Kim, S.; Guenther, A. B.; Goldstein, A. H.; Keutsch, F. N.; Springston, S. R.; Watson, T. B.; Artaxo, P.; Souza, R. A. F.; McKinney, K. A.; Martin, S. T. Isoprene Photo-Oxidation Products Quantify the Effect of Pollution on Hydroxyl Radicals over Amazonia. *Sci. Adv.* **2018**, *4* (4), eaar2547.

(39) Stull, R. B. *An Introduction to Boundary Layer Meteorology*; Springer, 1988.

(40) George, C.; Ammann, M.; D'Anna, B.; Donaldson, D. J.; Nizkorodov, S. A. Heterogeneous Photochemistry in the Atmosphere. *Chem. Rev.* **2015**, *115* (10), 4218−4258.

(41) Blando, J. D.; Turpin, B. J. Secondary Organic Aerosol Formation in Cloud and Fog Droplets: A Literature Evaluation of Plausibility. *Atmos. Environ.* **2000**, *34* (10), 1623−1632.

(42) Ervens, B. Progress and Problems in Modeling Chemical Processing in Cloud Droplets and Wet Aerosol Particles. In *Multiphase Environmental Chemistry in the Atmosphere*; ACS Symposium Series; American Chemical Society, 2018; Vol. 1299, pp 327−345. .

(43) Herckes, P.; Valsaraj, K. T.; Collett, J. L. A Review of Observations of Organic Matter in Fogs and Clouds: Origin, Processing and Fate. *Atmos. Res.* **2013**, *132−133*, 434−449.

(44) van Pinxteren, D.; Plewka, A.; Hofmann, D.; Müller, K.; Kramberger, H.; Svrcina, B.; Bächmann, K.; Jaeschke, W.; Mertes, S.; Collett, J. L.; Herrmann, H. Schmücke Hill Cap Cloud and Valley Stations Aerosol Characterisation during FEBUKO (II): Organic Compounds. *Atmos. Environ.* **2005**, *39* (23), 4305−4320.

(45) Decesari, S.; Facchini, M. C.; Fuzzi, S.; McFiggans, G. B.; Coe, H.; Bower, K. N. The Water-Soluble Organic Component of Size-Segregated Aerosol, Cloud Water and Wet Depositions from Jeju Island during ACE-Asia. *Atmos. Environ.* **2005**, *39* (2), 211−222.

(46) Lim, Y. B.; Tan, Y.; Perri, M. J.; Seitzinger, S. P.; Turpin, B. J. Aqueous Chemistry and Its Role in Secondary Organic Aerosol (SOA) Formation. *Atmos. Chem. Phys.* **2010**, *10* (21), 10521−10539.

(47) Carlton, A. G.; Wiedinmyer, C.; Kroll, J. H. A Review of Secondary Organic Aerosol (SOA) Formation from Isoprene. *Atmos. Chem. Phys.* **2009**, *9* (14), 4987−5005.

(48) Sareen, N.; Carlton, A. G.; Surratt, J. D.; Gold, A.; Lee, B.; Lopez-Hilfiker, F.; Mohr, C.; Thornton, J. A.; Zhang, Z.; Lim, Y. B.; Turpin, B. J. Identifying Precursors and Aqueous Organic Aerosol

Formation Pathways during the SOAS Campaign. *Atmos. Chem. Phys.* **2016**, *16* (22), 14409−14420.

(49) Petters, S. S.; Hilditch, T. G.; Tomaz, S.; Miles, R. E. H.; Reid, J. P.; Turpin, B. J. Volatility Change During Droplet Evaporation of Pyruvic Acid. *ACS Earth Space Chem.* **2020**, *4*, 741.

(50) Tsui, W. G.; Woo, J. L.; McNeill, V. F. Impact of Aerosol-Cloud Cycling on Aqueous Secondary Organic Aerosol Formation. *Atmosphere* **2019**, *10* (11), 666.

(51) Sareen, N.; Waxman, E. M.; Turpin, B. J.; Volkamer, R.; Carlton, A. G. Potential of Aerosol Liquid Water to Facilitate Organic Aerosol Formation: Assessing Knowledge Gaps about Precursors and Partitioning. *Environ. Sci. Technol.* **2017**, *51* (6), 3327−3335.

(52) Eddingsaas, N. C.; VanderVelde, D. G.; Wennberg, P. O. Kinetics and Products of the Acid-Catalyzed Ring-Opening of Atmospherically Relevant Butyl Epoxy Alcohols. *J. Phys. Chem. A* **2010**, *114* (31), 8106−8113.

(53) Pye, H. O. T.; Pinder, R. W.; Piletic, I. R.; Xie, Y.; Capps, S. L.; Lin, Y.-H.; Surratt, J. D.; Zhang, Z.; Gold, A.; Luecken, D. J.; Hutzell, W. T.; Jaoui, M.; Offenberg, J. H.; Kleindienst, T. E.; Lewandowski, M.; Edney, E. O. Epoxide Pathways Improve Model Predictions of Isoprene Markers and Reveal Key Role of Acidity in Aerosol Formation. *Environ. Sci. Technol.* **2013**, *47* (19), 11056−11064.

(54) Gaston, C. J.; Riedel, T. P.; Zhang, Z.; Gold, A.; Surratt, J. D.; Thornton, J. A. Reactive Uptake of an Isoprene-Derived Epoxydiol to Submicron Aerosol Particles. *Environ. Sci. Technol.* **2014**, *48* (19), 11178−11186.

(55) Nguyen, T. B.; Coggon, M. M.; Bates, K. H.; Zhang, X.; Schwantes, R. H.; Schilling, K. A.; Loza, C. L.; Flagan, R. C.; Wennberg, P. O.; Seinfeld, J. H. Organic Aerosol Formation from the Reactive Uptake of Isoprene Epoxydiols (IEPOX) onto Non-Acidified Inorganic Seeds. *Atmos. Chem. Phys.* **2014**, *14* (7), 3497−3510.

(56) Karambelas, A.; Pye, H. O. T.; Budisulistiorini, S. H.; Surratt, J. D.; Pinder, R. W. Contribution of Isoprene Epoxydiol to Urban Organic Aerosol: Evidence from Modeling and Measurements. *Environ. Sci. Technol. Lett.* **2014**, *1* (6), 278−283.

(57) Kampf, C. J.; Waxman, E. M.; Slowik, J. G.; Dommen, J.; Pfaffenberger, L.; Praplan, A. P.; Prévôt, A. S. H.; Baltensperger, U.; Hoffmann, T.; Volkamer, R. Effective Henry's Law Partitioning and the Salting Constant of Glyoxal in Aerosols Containing Sulfate. *Environ. Sci. Technol.* **2013**, *47* (9), 4236−4244.

(58) Ip, H. S. S.; Huang, X. H. H.; Yu, J. Z. Effective Henry's Law Constants of Glyoxal, Glyoxylic Acid, and Glycolic Acid. *Geophys. Res. Lett.* **2009**, *36* (1). DOI: 10.1029/2008GL036212.

(59) Kroll, J. H.; Ng, N. L.; Murphy, S. M.; Varutbangkul, V.; Flagan, R. C.; Seinfeld, J. H. Chamber Studies of Secondary Organic Aerosol Growth by Reactive Uptake of Simple Carbonyl Compounds. *J. Geophys. Res.* **2005**, *110* (D23). DOI: 10.1029/2005JD006004.

(60) Zhou, X.; Mopper, K. Apparent Partition Coefficients of 15 Carbonyl Compounds between Air and Seawater and between Air and Freshwater; Implications for Air-Sea Exchange. *Environ. Sci. Technol.* **1990**, *24* (12), 1864−1869.

(61) Sander, R. Compilation of Henry's Law Constants (Version 4.0) for Water as Solvent. *Atmos. Chem. Phys.* **2015**, *15* (8), 4399−4981.

(62) Betterton, E. A.; Hoffmann, M. R. Henry's Law Constants of Some Environmentally Important Aldehydes. *Environ. Sci. Technol.* **1988**, *22* (12), 1415−1418.

(63) Khan, I.; Brimblecombe, P. Henry's Law Constants of Low Molecular Weight (<130) Organic Acids. *J. Aerosol Sci.* **1992**, *23*, 897−900.

(64) Khan, I.; Brimblecombe, P.; Clegg, S. L. Solubilities of Pyruvic Acid and the Lower (C1-C6) Carboxylic Acids. Experimental Determination of Equilibrium Vapour Pressures above Pure Aqueous and Salt Solutions. *J. Atmos. Chem.* **1995**, *22* (3), 285−302.

(65) Khan, I.; Brmblecombe, P.; Clegg, S. L. The Henry's Law Constants of Pyruvic and Methacrylic Acids. *Environ. Technol.* **1992**, *13* (6), 587−593.

(66) LeClair, J. P.; Collett, J. L.; Mazzoleni, L. R. Fragmentation Analysis of Water-Soluble Atmospheric Organic Matter Using Ultrahigh-Resolution FT-ICR Mass Spectrometry. *Environ. Sci. Technol.* **2012**, *46* (8), 4312−4322.

(67) Altieri, K. E.; Turpin, B. J.; Seitzinger, S. P. Oligomers, Organosulfates, and Nitrooxy Organosulfates in Rainwater Identified by Ultra-High Resolution Electrospray Ionization FT-ICR Mass Spectrometry. *Atmos. Chem. Phys.* **2009**, *9* (7), 2533−2542.

(68) Pratt, K. A.; Fiddler, M. N.; Shepson, P. B.; Carlton, A. G.; Surratt, J. D. Organosulfates in Cloud Water above the Ozarks' Isoprene Source Region. *Atmos. Environ.* **2013**, *77*, 231−238.

(69) Mazzoleni, L. R.; Ehrmann, B. M.; Shen, X.; Marshall, A. G.; Collett, J. L. Water-Soluble Atmospheric Organic Matter in Fog: Exact Masses and Chemical Formula Identification by Ultrahigh-Resolution Fourier Transform Ion Cyclotron Resonance Mass Spectrometry. *Environ. Sci. Technol.* **2010**, *44* (10), 3690−3697.

(70) Spolnik, G.; Wach, P.; Rudziński, K. J.; Szmigielski, R.; Danikiewicz, W. Tracing the Biogenic Secondary Organic Aerosol Markers in Rain, Snow and Hail. *Chemosphere* **2020**, *251*, 126439.

(71) Lin, Y.-H.; Zhang, H.; Pye, H. O. T.; Zhang, Z.; Marth, W. J.; Park, S.; Arashiro, M.; Cui, T.; Budisulistiorini, S. H.; Sexton, K. G.; Vizuete, W.; Xie, Y.; Luecken, D. J.; Piletic, I. R.; Edney, E. O.; Bartolotti, L. J.; Gold, A.; Surratt, J. D. Epoxide as a Precursor to Secondary Organic Aerosol Formation from Isoprene Photooxidation in the Presence of Nitrogen Oxides. *Proc. Natl. Acad. Sci. U. S. A.* **2013**, *110* (17), 6718−6723.

(72) Otto, T.; Schaefer, T.; Herrmann, H. Aqueous-Phase Oxidation of Cis-*β*-Isoprene Epoxydiol by Hydroxyl Radicals and Its Impact on Atmospheric Isoprene Processing. *J. Phys. Chem. A* **2019**, *123* (49), 10599−10608.

(73) Chen, Y.; Zhang, Y.; Lambe, A. T.; Xu, R.; Lei, Z.; Olson, N. E.; Zhang, Z.; Szalkowski, T.; Cui, T.; Vizuete, W.; Gold, A.; Turpin, B. J.; Ault, A. P.; Chan, M. N.; Surratt, J. D. Heterogeneous Hydroxyl Radical Oxidation of Isoprene Epoxydiol-Derived Methyltetrol Sulfates: Plausible Formation Mechanisms of Previously Unexplained Organosulfates in Ambient Fine Aerosols. *Environ. Sci. Technol. Lett.* **2020**, *7*, 460.

(74) Minerath, E. C.; Elrod, M. J. Assessing the Potential for Diol and Hydroxy Sulfate Ester Formation from the Reaction of Epoxides in Tropospheric Aerosols. *Environ. Sci. Technol.* **2009**, *43* (5), 1386−1392.

(75) Cash, J. M.; Heal, M. R.; Langford, B.; Drewer, J. A Review of Stereochemical Implications in the Generation of Secondary Organic Aerosol from Isoprene Oxidation. *Environ. Sci. Process. Impacts* **2016**, *18* (11), 1369−1380.

(76) Fredenslund, A.; Jones, R. L.; Prausnitz, J. M. Group-Contribution Estimation of Activity Coefficients in Nonideal Liquid Mixtures. *AIChE J.* **1975**, *21* (6), 1086−1099.

(77) Suda, S. R.; Petters, M. D.; Yeh, G. K.; Strollo, C.; Matsunaga, A.; Faulhaber, A.; Ziemann, P. J.; Prenni, A. J.; Carrico, C. M.; Sullivan, R. C.; Kreidenweis, S. M. Influence of Functional Groups on Organic Aerosol Cloud Condensation Nucleus Activity. *Environ. Sci. Technol.* **2014**, *48* (17), 10182−10190.

(78) Petters, S. S.; Pagonis, D.; Claflin, M. S.; Levin, E. J. T.; Petters, M. D.; Ziemann, P. J.; Kreidenweis, S. M. Hygroscopicity of Organic Compounds as a Function of Carbon Chain Length and Carboxyl, Hydroperoxy, and Carbonyl Functional Groups. *J. Phys. Chem. A* **2017**, *121* (27), 5164−5174.

(79) Rothfuss, N. E.; Petters, M. D. Influence of Functional Groups on the Viscosity of Organic Aerosol. *Environ. Sci. Technol.* **2017**, *51* (1), 271−279.

(80) Darer, A. I.; Cole-Filipiak, N. C.; O'Connor, A. E.; Elrod, M. J. Formation and Stability of Atmospherically Relevant Isoprene-Derived Organosulfates and Organonitrates. *Environ. Sci. Technol.* **2011**, *45* (5), 1895−1902.

(81) Lam, H. K.; Kwong, K. C.; Poon, H. Y.; Davies, J. F.; Zhang, Z.; Gold, A.; Surratt, J. D.; Chan, M. N. Heterogeneous OH Oxidation of Isoprene-Epoxydiol-Derived Organosulfates: Kinetics, Chemistry and Formation of Inorganic Sulfate. *Atmos. Chem. Phys.* **2019**, *19* (4), 2433−2440.

(82) Petters, S. S.; Kreidenweis, S. M.; Grieshop, A. P.; Ziemann, P. J.; Petters, M. D. Temperature- and Humidity-Dependent Phase States of Secondary Organic Aerosols. *Geophys. Res. Lett.* **2019**, *46* (2), 1005−1013.

(83) Zhang, Z.; Lin, Y.-H.; Zhang, H.; Surratt, J. D.; Ball, L. M.; Gold, A. Technical Note: Synthesis of Isoprene Atmospheric Oxidation Products: Isomeric Epoxydiols and the Rearrangement Products Cis- and Trans-3-Methyl-3,4-Dihydroxytetrahydrofuran. *Atmos. Chem. Phys.* **2012**, *12* (18), 8529−8535.

(84) Bondy, A. L.; Craig, R. L.; Zhang, Z.; Gold, A.; Surratt, J. D.; Ault, A. P. Isoprene-Derived Organosulfates: Vibrational Mode Analysis by Raman Spectroscopy, Acidity-Dependent Spectral Modes, and Observation in Individual Atmospheric Particles. *J. Phys. Chem. A* **2018**, *122* (1), 303−315.

(85) McNeill, V. F.; Woo, J. L.; Kim, D. D.; Schwier, A. N.; Wannell, N. J.; Sumner, A. J.; Barakat, J. M. Aqueous-Phase Secondary Organic Aerosol and Organosulfate Formation in Atmospheric Aerosols: A Modeling Study. *Environ. Sci. Technol.* **2012**, *46* (15), 8075−8081.

(86) McNeill, V. F. Aqueous Organic Chemistry in the Atmosphere: Sources and Chemical Processing of Organic Aerosols. *Environ. Sci. Technol.* **2015**, *49* (3), 1237−1244.

(87) van Pinxteren, D.; Fomba, K. W.; Mertes, S.; Müller, K.; Spindler, G.; Schneider, J.; Lee, T.; Collett, J. L.; Herrmann, H. Cloud Water Composition during HCCT-2010: Scavenging Efficiencies, Solute Concentrations, and Droplet Size Dependence of Inorganic Ions and Dissolved Organic Carbon. *Atmos. Chem. Phys.* **2016**, *16* (5), 3185−3205.

(88) Schwab, J. J.; Casson, P.; Brandt, R.; Husain, L.; Dutkewicz, V.; Wolfe, D.; Demerjian, K. L.; Civerolo, K. L.; Rattigan, O. V.; Felton, H. D.; Dukett, J. E. Atmospheric Chemistry Measurements at Whiteface Mountain, NY: Cloud Water Chemistry, Precipitation Chemistry, and Particulate Matter. *Aerosol Air Qual. Res.* **2016**, *16* (3), 841−854.

(89) Clegg, S. L.; Brimblecombe, P.; Wexler, A. S. Thermodynamic Model of the System H^+− NH_4^+− Na^+− $SO_4^{2−}$− $NO_3^−$− $Cl^−$− H_2O at 298.15 K. *J. Phys. Chem. A* **1998**, *102* (12), 2155−2171.

(90) Wexler, A. S.; Clegg, S. L. Atmospheric Aerosol Models for Systems Including the Ions H^+, NH_4^+, Na^+, $SO_4^{2−}$, $NO_3^−$, $Cl^−$, Br−, and H_2O. *J. Geophys. Res.* **2002**, *107* (D14), 4207.

(91) Wiberg, K. B. The Deuterium Isotope Effect. *Chem. Rev.* **1955**, *55* (4), 713−743.

(92) Swain, C. G. A Transition from Specific Oxonium-Ion Catalysis to General Acid Catalysis1. *J. Am. Chem. Soc.* **1952**, *74* (16), 4108−4110.

(93) Whalen, D. L. Mechanisms of Hydrolysis and Rearrangements of Epoxides. In *Adv. Phys. Org. Chem.*; Richard, J. P., Ed.; Academic Press, 2005; Vol. 40, pp 247−298. .

(94) Whalen, D. L.; Ross, A. M.; Montemarano, J. A.; Thakker, D. R.; Yagi, H.; Jerina, D. M. General Acid Catalysis in the Hydrolysis of Benzo[a]Pyrene 7,8-Diol 9,10-Epoxides. *J. Am. Chem. Soc.* **1979**, *101* (17), 5086−5088.

(95) Nozière, B.; Fache, F.; Maxut, A.; Fenet, B.; Baudouin, A.; Fine, L.; Ferronato, C. The Hydrolysis of Epoxides Catalyzed by Inorganic Ammonium Salts in Water: Kinetic Evidence for Hydrogen Bond Catalysis. *Phys. Chem. Chem. Phys.* **2018**, *20* (3), 1583−1590.

(96) Mabey, W.; Mill, T. Critical Review of Hydrolysis of Organic Compounds in Water under Environmental Conditions. *J. Phys. Chem. Ref. Data* **1978**, *7* (2), 383−415.

(97) Long, F. A.; Pritchard, J. G. Hydrolysis of Substituted Ethylene Oxides in H2O18 Solutions. *J. Am. Chem. Soc.* **1956**, *78* (12), 2663−2667.

(98) Pritchard, J. G.; Long, F. A. Kinetics and Mechanism of the Acid-Catalyzed Hydrolysis of Substituted Ethylene Oxides. *J. Am. Chem. Soc.* **1956**, *78* (12), 2667−2670.

(99) Mori, A. L.; Schaleger, L. L. Kinetics and Mechanism of Epoxy Ether Hydrolysis. II. Mechanism of Ring Cleavage. *J. Am. Chem. Soc.* **1972**, *94* (14), 5039−5043.

(100) Bunton, C. A.; Shiner, V. J. Isotope Effects in Deuterium Oxide Solution. I. Acid-Base Equilibria. *J. Am. Chem. Soc.* **1961**, *83* (1), 42−47.

(101) Isbell, H. S.; Pigman, W. Mutarotation of Sugars in Solution: PART II: Catalytic Processes, Isotope Effects, Reaction Mechanisms, and Biochemical Aspects. In *Adv. Carbohydr. Chem. Biochem.*; Wolfrom, M. L., Tipson, R. S., Horton, D., Eds.; Academic Press, 1969; Vol. 24, pp 13−65. .

(102) Piletic, I. R.; Edney, E. O.; Bartolotti, L. J. A Computational Study of Acid Catalyzed Aerosol Reactions of Atmospherically Relevant Epoxides. *Phys. Chem. Chem. Phys.* **2013**, *15* (41), 18065−18076.

(103) Perdoncin, G.; Scorrano, G. Protonation Equilibria in Water at Several Temperatures of Alcohols, Ethers, Acetone, Dimethyl Sulfide, and Dimethyl Sulfoxide. *J. Am. Chem. Soc.* **1977**, *99* (21), 6983−6986.

(104) Aoki, E.; Sarrimanolis, J. N.; Lyon, S. A.; Elrod, M. J. Determining the Relative Reactivity of Sulfate, Bisulfate and Organosulfates with Epoxides on Secondary Organic Aerosol. *ACS Earth Space Chem.* **2020**, *4*, 1793.

(105) Pritchard, J. G.; Siddiqui, I. A. Activation Parameters and Mechanism of the Acid-Catalysed Hydrolysis of Epoxides. *J. Chem. Soc., Perkin Trans. 2* **1973**, No. 4, 452−457.

(106) Prausnitz, J. M.; Lichtenthaler, R. N.; de Azevedo, E. G. *Molecular Thermodynamics of Fluid-Phase Equilibria*, 3rd ed.; Prentice Hall: Upper Saddle River, New Jersey, USA, 1999.

(107) Cole-Filipiak, N. C.; O'Connor, A. E.; Elrod, M. J. Kinetics of the Hydrolysis of Atmospherically Relevant Isoprene-Derived Hydroxy Epoxides. *Environ. Sci. Technol.* **2010**, *44* (17), 6718−6723.

(108) Link, M. F.; Nguyen, T. B.; Bates, K.; Müller, J.-F.; Farmer, D. K. Can Isoprene Oxidation Explain High Concentrations of Atmospheric Formic and Acetic Acid over Forests? *ACS Earth Space Chem.* **2020**, *4* (5), 730−740.

(109) Birdsall, A. W.; Miner, C. R.; Mael, L. E.; Elrod, M. J. Mechanistic Study of Secondary Organic Aerosol Components Formed from Nucleophilic Addition Reactions of Methacrylic Acid Epoxide. *Atmos. Chem. Phys.* **2014**, *14* (23), 12951−12964.

(110) Nobes, R. H.; Radom, L. Structures and Relative Energies of Gas Phase $[C_3H_7O]^+$ Ions. *Org. Mass Spectrom.* **1984**, *19* (8), 385−393.

(111) Totobenazara, J.; Haroun, H.; Rémond, J.; Adil, K.; Dénès, F.; Lebreton, J.; Gaulon-Nourry, C.; Gosselin, P. Tandem Payne/Meinwald versus Meinwald Rearrangements on the α-Hydroxy- or α-Silyloxy-Spiro Epoxide Skeleton. *Org. Biomol. Chem.* **2012**, *10* (3), 502−505.

(112) Lee, A. K. Y.; Zhao, R.; Li, R.; Liggio, J.; Li, S.-M.; Abbatt, J. P. D. Formation of Light Absorbing Organo-Nitrogen Species from Evaporation of Droplets Containing Glyoxal and Ammonium Sulfate. *Environ. Sci. Technol.* **2013**, *47* (22), 12819−12826.

(113) Bain, R. M.; Pulliam, C. J.; Thery, F.; Cooks, R. G. Accelerated Chemical Reactions and Organic Synthesis in Leidenfrost Droplets. *Angew. Chem., Int. Ed.* **2016**, *55* (35), 10478−10482.

(114) Huang, Y.; Zhang, R.; Li, K.; Cheng, Z.; Zhong, G.; Zhang, G.; Li, J. Experimental Study on the Role of Sedimentation and Degradation Processes on Atmospheric Deposition of Persistent Organic Pollutants in a Subtropical Water Column. *Environ. Sci. Technol.* **2017**, *51* (8), 4424−4433.